TULP1 Mutations Causing Early-Onset Retinal Degeneration: Preserved but Insensitive Macular Cones

Samuel G. Jacobson,[1] Artur V. Cideciyan,[1] Wei Chieh Huang,[1] Alexander Sumaroka,[1] Alejandro J. Roman,[1] Sharon B. Schwartz,[1] Xunda Luo,[1] Rebecca Sheplock,[1] Joanna M. Dauber,[1] Malgorzata Swider,[1] and Edwin M. Stone[2,3]

[1]Scheie Eye Institute, Department of Ophthalmology, Perelman School of Medicine, University of Pennsylvania, Philadelphia, Pennsylvania, United States
[2]Department of Ophthalmology, University of Iowa Carver College of Medicine, Iowa City, Iowa, United States
[3]Howard Hughes Medical Institute, Iowa City, Iowa, United States

Correspondence: Samuel G. Jacobson, Scheie Eye Institute, University of Pennsylvania, 51 N. 39th Street, Philadelphia, PA 19104, USA; jacobsos@mail.med.upenn.edu.

Submitted: April 10, 2014
Accepted: July 13, 2014

Citation: Jacobson SG, Cideciyan AV, Huang WC, et al. *TULP1* mutations causing early-onset retinal degeneration: preserved but insensitive macular cones. *Invest Ophthalmol Vis Sci*. 2014;55:5354–5364. DOI:10.1167/iovs.14-14570

Purpose. To investigate visual function and outer and inner retinal structure in the rare form of retinal degeneration (RD) caused by *TULP1* (*tubby-like protein 1*) mutations.

Methods. Retinal degeneration patients with *TULP1* mutations ($n = 5$; age range, 5–36 years) were studied by kinetic and chromatic static perimetry, en face autofluorescence imaging, and spectral-domain optical coherence tomography (OCT) scans. Outer and inner retinal laminar thickness were measured and mapped across the central retina. Comparisons were made with results from patients with RD associated with four ciliopathy genotypes (*MAK*, *RPGR*, *BBS1*, and *USH2A*).

Results. The *TULP1*-RD patients were severely affected already in the first decade of life and there was rapidly progressive visual loss. No evidence of rod function was present at any age. Small central islands showed melanized retinal pigment epithelium by autofluorescence imaging and well-preserved photoreceptor laminar thickness by OCT imaging. There was extracentral loss of laminar architecture and increased inner retinal thickening. Structure-function relationships in residual foveal cone islands were made in *TULP1*-RD patients and in other retinopathies considered ciliopathies. Patients with *TULP1*-RD, unlike the others, had greater dysfunction for the degree of foveal structural preservation.

Conclusions. Retinal degeneration with *TULP1* mutations leads to a small central island of residual foveal cones at early ages. These cones are less sensitive than expected from the residual structure. The human phenotype is consistent with experimental evidence in the *Tulp1* knockout mouse model that visual dysfunction could be complicated by abnormal processes proximal to cone outer segments.

Keywords: cilia, optical coherence tomography, Leber congenital amaurosis, rod, cone

The discovery of the tubby gene family[1] and disease association of the gene encoding tubby-like protein 1 (*TULP1*) with retinitis pigmentosa (RP) 14, an autosomal recessive (ar) retinal degeneration locus on chromosome 6p, occurred more than a decade ago.[2–6] This was followed by reports of patients with *TULP1* mutations and clinical descriptions that continued to describe the disease as arRP or used alternative diagnoses such as early-onset retinal degeneration (EORD) or Leber congenital amaurosis (LCA).[7–15]

What do we know about retinal disease mechanisms in TULP1 deficiency? The *tulp1* knockout mouse (*tulp1*$^{-/-}$) shows progressive loss of rod and cone photoreceptor nuclei over the first 4 to 5 months of life. Tulp1 is located in the photoreceptor inner segments of wild-type mice. Accumulation of vesicles in the interphotoreceptor matrix was noted in *tulp1*$^{-/-}$ mice and attributed to transport abnormalities from inner segment to outer segment.[16–18] It has also been suggested that Tulp1 is critical for development of the photoreceptor synapse[19] and may have a role in phagocytosis.[20]

Any ongoing or planned therapeutic directions for forms of EORD or LCA depend on whether there are detectable photoreceptors remaining in the retinas of molecularly clarified patients.[21,22] Photoreceptor laminar integrity as measured by optical coherence tomography (OCT) can provide the information suggesting which of the therapeutic directions would be most appropriate to consider and develop in the future for patients with *TULP1*-associated RD. We studied a cohort of patients with *TULP1* mutations and determined retinal laminar architecture as well as visual function to provide information about treatment potential for this disease. The wider question posed was whether the pattern of phenotype results in patients with *TULP1* mutations was different from those of other retinal degenerations considered ciliopathies.[23–25]

Methods

Subjects

There were five RD patients, representing four families, with *TULP1* mutations and 32 patients with other molecularly

Table. Clinical and Molecular Characteristics of the Patients

Patient	Age at Visits, y	Sex	Allele 1/Allele 2	Visual Acuity† RE	Visual Acuity† LE	Refraction‡ RE	Refraction‡ LE	Previous Report§
TULP1||								
P1¶	4,10,15	F	p.Q301Ter/p.Q301Ter	20/160	20/125	−1.25	−1.25	
P2¶	9,15,19	M	p.Q301Ter/p.Q301Ter	20/200	20/200	+6.00	+6.00	
P3	17,25	F	p.G368W/p.D355V	20/80	20/80	Plano	+0.50	
P4	27,36	M	p.R400Q/p.Y321D	HM	HM	−1.25	−1.50	
P5	28,33	F	p.R400W/p.R400W	20/100	20/100	+5.75	+6.75	
MAK#								
P6	55	M	p.K429 insAlu_353bp/p.K429 insAlu_353bp	20/20	20/25	−1.50	−2.50	
P7**	59	F	p.K429 insAlu_353bp/p.K429 insAlu_353bp	20/40	20/63	−7.00	−8.00	P6[54]
P8**	72	F	p.K429 insAlu_353bp/p.K429 insAlu_353bp	20/25	20/20	Plano	Plano	P9[54]
RPGR‡‡								
P9	7	M	p.S551fs	20/30	20/30	−0.75	−0.75	
P10	15	M	p.E746fs	20/25	20/20	−3.25	−3.75	P16, F5[76]
P11	17	M	p.E802fs	20/50	20/32	+1.75	+2.75	
P12	22	M	p.E746fs	20/40	20/25	−2.00	−2.50	P29, F15[76]
P13	25	M	p.G743Ter	20/50	20/30	+0.75	+0.75	P19, F7[76]
P14	27	M	p.E872Ter	20/32	20/40	−4.50	−5.25	P20, F8[76]
P15	28	M	p.E915Ter	20/25	20/25	−3.25	−4.25	P30, F16[76]
P16	38	M	p.G702fs	20/63	20/50	−1.50	−1.50	P18, F6[76]
P17	42	M	p.E802fs	20/32	20/32	−5.25	−4.00	P5, F1[76]
P18	45	M	p.E802fs	20/100	20/40	−4.25	−3.00	
P19	45	M	p.L460fs	20/32	20/25	+2.25	+1.75	
P20	46	M	p.E956fs	20/160	20/160	−0.75	−0.50	
P21	47	M	p.E839fs	20/300	20/150	−2.00	−2.00	
P22	51	M	p.E802fs	20/70	20/150	−10.50	−3.75	P33, F19[76]
P23§§	53	M	p.E754Ter	HM	HM	NA	NA	P13, F4[76]
P24§§	61	M	p.E754Ter	HM	HM	−6.50	−6.00	P14, F4[76]
BBS1¶¶								
P25	16	M	p.M390R/p.M390R	20/20	20/20	−1.50	−1.50	P3[77]
P26	17	M	p.R277K/p.I1389 del	20/1000	HM	Plano	Plano	
P27	21	M	p.M390R/p.R483Ter	20/150	20/150	+0.75	+0.75	
P28	22	F	p.M390R/p.M390R	20/32	20/32	−4.00	−4.75	
P29	24	F	p.M390R/p.M390R	20/63	20/50	−3.25	−3.50	P1[77]
P30	27	M	p.M390R/p.M390R	10/200	12/200	−3.50	−3.50	P5[77]
P31	29	F	p.M390R/p.M390R	20/80	20/100	−4.75	−3.75	
USH2A##								
P32	24	F	p.C759F/p.W3955Ter	20/20	20/20	−0.25	−0.25	P2[58]; F12, P1[78]
P33	31	M	p.Y1838Ter/p.C2128F	20/32	20/200	−1.50	−1.50	
P34	41	M	p.E767fs/p.N405fs	20/50	20/25	−0.25	Plano	P3[58]; F4, P1[79]
P35	43	F	p.C759F/p.V218E	20/20	20/20	−0.50	−0.50	P5[58]; F16, P1[78]
P36	62	M	p.C759F/p.C759F	20/40	20/40	+0.75	+0.50	
P37	81	F	p.E767fs/p.E767fs	LP	LP	+13.75	+14.00	

HM, hand motions; LP, light perception; NA, not available; RE; right eye; LE, left eye. Novel mutation indicated in bold italics.

† Best corrected visual acuity at first visit.

‡ Spherical equivalent.

§ Previous reports of phenotype and/or genotype, but neither the same data nor at same disease stage or patient age: Stone et al.,[54] Huang et al.,[76] Azari et al.,[77] Jacobson et al.,[58] Herrera et al.,[78] and Schwartz et al.[79]

|| Numbering according to GenBank accession number NM_003322 starting at the translation initiation codon.

¶ §§Patients are siblings.

Numbering according to GenBank accession number NM_005906.4 starting at the translation initiation codon.

** Patients are cousins.

‡‡ Numbering according to GenBank accession number NM_001034853.1 starting at the translation initiation codon.

¶¶ Numbering according to GenBank accession number NM_024649 starting at the translation initiation codon.

Numbering according to GenBank accession number NM_206933.2 starting at the translation initiation codon.

clarified retinal degenerations (Table). All patients (and normal subjects) underwent a complete eye examination. Informed consent was obtained from all subjects. Procedures adhered to the Declaration of Helsinki and were approved by the institutional review board.

Imaging Studies—OCT

Retinal OCT cross-sections were obtained with a spectral-domain OCT system (RTVue-100; Optovue Inc., Fremont, CA, USA, and Bioptigen, Inc., Durham, NC, USA) in all *TULP1*-RD

patients and most other ciliopathy patients studied. Data from a limited number of ciliopathy patients were collected using time-domain OCT instruments (OCT1, OCT3; Carl Zeiss Meditec, Dublin, CA, USA). Scans from OCT were acquired along the horizontal and vertical meridians with fovea at the center. Patient fixation was then shifted along horizontal (nasal-temporal) and vertical (inferior-superior) axes to permit a maximum of 60°-wide coverage. Postacquisition data analysis was performed with custom programs (MATLAB 7.5; MathWorks, Natick, MA, USA). Horizontal or vertical central scans and those nasal and temporal or inferior and superior to the fovea were digitally merged by custom programs. Longitudinal reflectivity profiles (LRPs) making up the scans of the merged images were aligned manually by straightening the RPE reflection. In normal subjects, the signal corresponding to the RPE was assumed to be the most scleral peak within the multipeaked scattering signal complex deep in the retina. In abnormal retinae, the presumed RPE peak was sometimes the only signal peak deep in the retina or could be accompanied by other major peaks. In the latter case, the RPE peak was specified manually by considering the properties of the backscattering signal originating from layers vitreal and scleral to it.

Outer nuclear layer (ONL) thickness was determined manually between the OPL (outer plexiform layer) and OLM (outer limiting membrane) peaks using both signal intensity and slope information.[21] A broad hyperscattering region originating from the Henle fiber layer (HFL) can appear scleral to the OPL and complicate measurements of ONL thickness. Visibility of this HFL layer changes with the angle of incidence of imaging rays.[26,27] The choice of OPL/ONL boundary in the present study is vitreal to the HFL reflection and our definition of ONL thickness includes the anatomical layers encompassing both photoreceptor nuclei and HFL.[28] Inner retinal thickness was defined as the distance from ILM to the vitreal boundary of OPL.[21,29,30] The normal ranges of ONL and inner retinal thickness were determined from 15 normal subjects (aged 8–62 years).

Foveal ONL and cone outer segment (COS) thicknesses were measured from three OCT scans through the fovea obtained at the same visit in patients with *TULP1*-RD and compared with measurements in groups of patients with four other genotypes. No patients with CME (cystoid macular edema) were included in the analyses. The outer retinal sublaminae were quantified according to our previous work[30–36] and those of others[37,38] and were consistent with hypotheses on the correspondence between OCT signals and histologically defined layers[29,39,40] and interpretations of ultrahigh resolution adaptive optics OCT scans.[41,42] These structural data (as the product of ONL and COS thickness) were compared with foveal function and a normal data set with both measurements was used ($n = 11$, ages 26-62).

Raster scans (6×6 mm) were used for topographic analysis of ONL and inner retinal thicknesses. The location and orientation of each scan relative to fundus features (blood vessels, optic nerve head) were determined using en face images. Longitudinal reflectivity profiles making up the OCT scans were allotted to regularly spaced bins in a rectangular coordinate system centered at the fovea; the waveforms in each bin were aligned and averaged. The measured thicknesses were mapped to a pseudo-color scale; missing data were interpolated bilinearly; and fundus landmarks were overlaid for reference. Normal data ($n = 5$, aged 23–45 years) for ONL and inner retinal thickness were compared with those of the patients.

Imaging Studies—Autofluorescence

En face imaging was performed with a confocal scanning laser ophthalmoscope (HRA2 or Spectralis; Heidelberg Engineering GmbH, Heidelberg, Germany) as previously published.[33,43] Retinal and subretinal features were imaged with 820 nm near-infrared (NIR) light in the reflectance (REF) mode. Health of the RPE was estimated with a reduced-illuminance autofluorescence imaging (RAFI) method using either 790 nm NIR excitation or 488 nm short-wavelength (SW) excitation. NIR-RAFI and SW-RAFI images were obtained with a fixed sensitivity setting (95% for HRA2 and 105% for Spectralis). Images for NIR-REF, NIR-RAFI, and SW-RAFI were captured in the "high-speed" mode where retinal regions ($30° \times 30°$ square or 55° diameter circular) were sampled onto a 768×768 pixel image. Automatic real-time averaging feature of the manufacturer's software was used to average 21 frames. For SW-RAFI, macular images were obtained; for NIR-REF and NIR-RAFI overlapping neighboring regions were digitally stitched by manually specifying corresponding retinal landmark pairs in order to generate wide angle composite images.

Visual Function

Two-color dark-adapted static perimetry was used to quantify rod- and cone-mediated visual function.[44] Sensitivities were measured at 2° intervals (1.7° diameter target; 200-ms duration stimulus) along the horizontal meridian.[45,46] Mediation by rod or cone photoreceptors was determined by comparison of sensitivity with a 500-nm stimulus to results using a 650-nm target.[44,45] Full field sensitivity testing (FST) was performed for the *TULP1*-RD patients,[45,47] as was full field ERG using International Society for Clinical Electrophysiology standard stimuli.[48]

Results

Clinical Features and Visual Function in *TULP1*-RD

All patients with *TULP1* mutations had a history of childhood-onset night vision disturbances, impaired visual acuity and clumsiness in mobility suggesting peripheral visual field problems. Visual acuities were no better than 20/80 on first visits and there was no common refractive error (Table). Nystagmus to varying degrees was present in all but patient 3 (P3). Funduscopic features outside the central retina ranged from no evident pigment migration (P1 at ages 5–15; P2 at age 9) to rare bone spicule-like pigment (P2 at ages 15 and 19; P3 at ages 17 and 25; P4 at ages 27 and 36) to dense pigmentary retinopathy (P5 at ages 28 and 33). Most patients had a granular appearance to the macula. Optic nerves had waxy pallor and P3 had disc drusen.

Full field ERGs showed no detectable responses to all stimuli in the five patients (at our earliest visits); those whom we first examined in the second and third decades of life had no detectable ERGs in childhood (by historical records). Kinetic and static chromatic perimetry results are shown (Fig. 1). At age 4, P1 was able to perform the task and a nearly full field was detected with a large bright target (V-4e). Subsequent fields at approximately 5 year intervals in P1 (ages 10 and 15) were reduced to small central islands with no detectable responding in the periphery. P2, the older brother of P1, had only a central island at age 9; there was no detectable field with this method at later visits (ages 15 and 19). At age 17, P3 had a central island connected to a temporal peripheral island along the horizontal meridian. On examination 8 years later at age 25, the general shape of the island was maintained but the extent was reduced. At age 27, P4 had a central island, but there was no detectable field at age 36. At ages 28 and 33, P5 retained a central island.

Investigative Ophthalmology & Visual Science

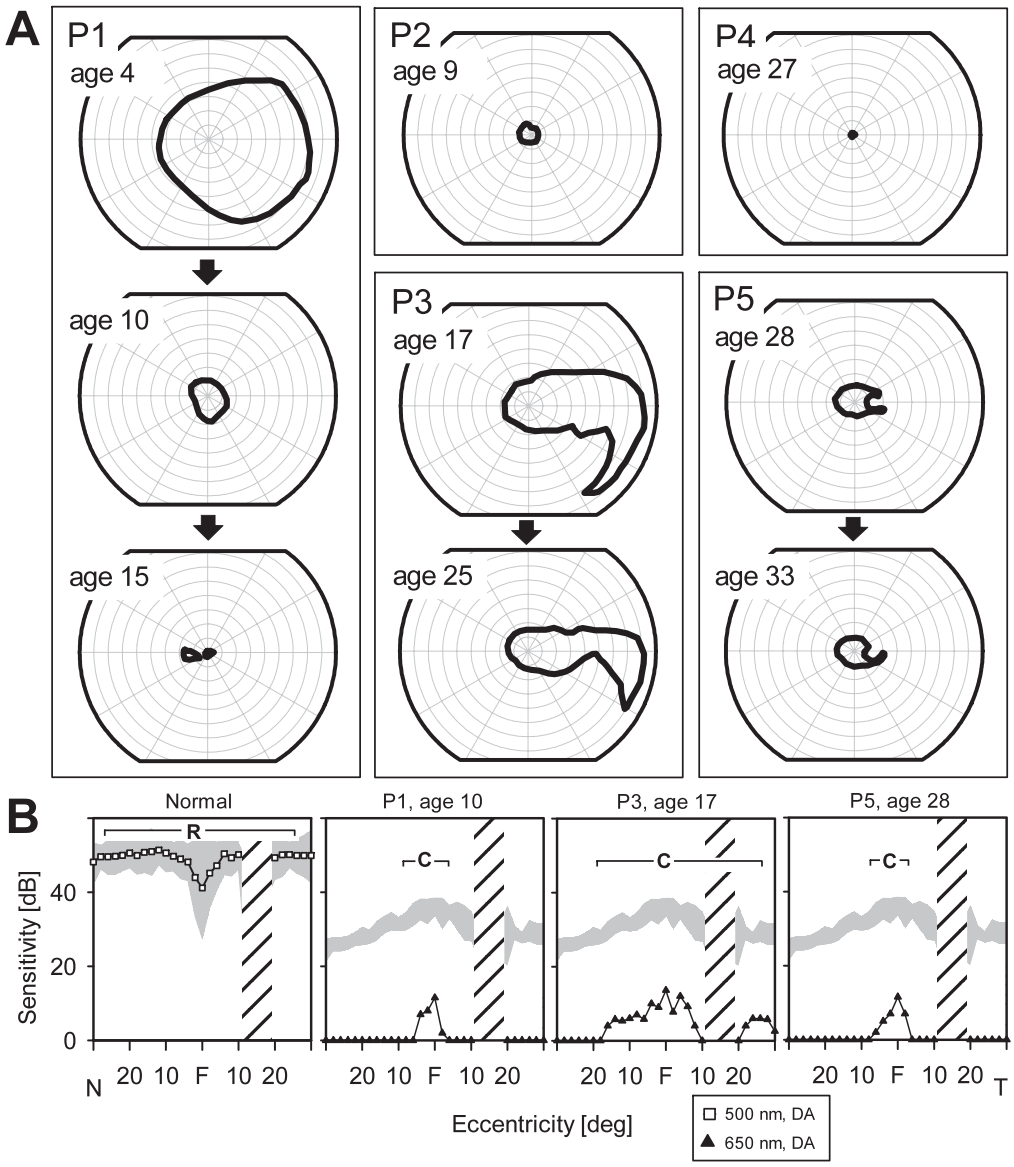

Figure 1. Visual function in *TULP1*-RD. (**A**) Kinetic perimetry (using V-4e test target) in the five patients (only one eye shown, and all represented as right eyes). Serial data are shown for P1, P3, and P5 at different ages (*arrows*). (**B**) Dark-adapted sensitivities at loci along the horizontal meridian in a normal subject and in P1, P3, and P5 using 500 (*squares*) and 650 nm (*triangles*) stimuli. Photoreceptor mediation at each locus, based on the sensitivity difference between the two colors, is given at the top of the graphs: *Gray shading* in the normal profile represents the normal limits (mean ± 2 SD) for rod-mediated function using the 500-nm stimulus. The *gray shading* in the patient profiles represents the normal limits for the 650-nm stimulus at cone plateau. Hatched area is region around and including the physiological blind spot. C, cone-mediated; F, fovea; N, nasal visual field; R, rod-mediated; T, temporal visual field.

Dark-adapted chromatic sensitivities to 500 and 650 nm stimuli were measurable in three patients (P1, P3, P5); sensitivity differences between the two colors were used to determine whether the vision was mediated by rods or cones. Unlike the normal rod-mediated results across 60° of the horizontal meridian (Fig. 1B, left), P1 and P5 had no detectable rod function but there were cone-mediated islands that were a few degrees in extent and severely reduced in function (Fig. 1B). Patient 3 also had no measurable rod function; and, as suggested by the kinetic perimetry results at the same age (Fig. 1A), cone function was detectable over retinal areas nasal to the optic disc. There were no responses to stimuli projected outside the central field; this indicated a peripheral field loss of 4 to 5 log units of rod function and 1 to 2 log units of cone function and was consistent with the nondetectable ERGs. Full-field sensitivity test results indicated approximately 5 log units of sensitivity loss and only cone-mediated function detectable.

En Face Imaging

Retinas of *TULP1*-RD P1, P2, and P3 showed en face imaging features (Fig. 2) generally similar to those seen in patients with retinitis pigmentosa.[33] Specifically, there was a central region of retained RPE melanization visible as a high signal on NIR-RAFI. The extent of this region was smallest in P1 at age 15 (Fig. 2B, ~4° diameter); largest in P2 at age 19 (Fig. 2C, ~8° diameter); and intermediate in P3 at age 25 (Fig. 2D, ~6° diameter). In P1 and P3, the centrally retained region

Investigative Ophthalmology & Visual Science

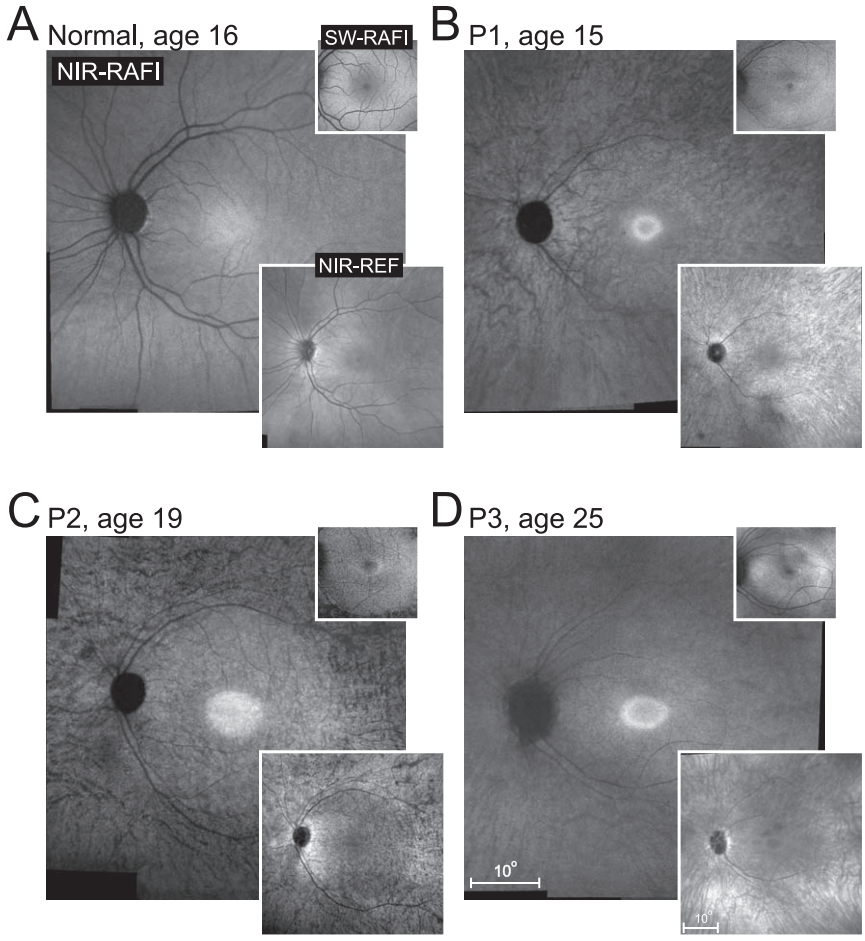

Figure 2. Digitally stitched wide-field NIR-RAFI results of a representative normal subject compared with three *TULP1*-RD patients. *Upper insets*, SW-RAFI, *lower insets*, NIR-REF images in the same eyes. (**A**) Results of NIR-RAFI of the 16 year-old normal subject demonstrate higher signal near the fovea smoothly transitioning to a lower signal in the pericentral and midperipheral regions. Blood vessels and the optic nerve appear dark. The SW-RAFI shows central depression corresponding to the macular pigment absorption. (**B**–**D**) The NIR-RAFI of *TULP1*-RD patients P1, P2, and P3 demonstrate relative hyperautofluorescence at or near the foveal region surrounded by lower signal and visibility of choroidal pattern of blood vessels implying partial depigmentation of the RPE. Results of SW-RAFI (*upper insets*) show retained RPE lipofuscin across all maculas. In P1, NIR reflectance image (*lower inset*) shows a distinctly demarcated elliptical region of ~4° diameter surrounding the fovea; P2 and P3 do not demonstrate evidence of this feature. All images are shown as equivalent left eyes and contrast stretched for visibility of features. Pair of calibrations shown in (**D**) apply to all panels; both *upper* and *lower insets* are displayed at the same magnification.

demonstrated a hyperautofluorescent ring on NIR-RAFI (Figs. 2B, 2D); and in P2, there was a hyperautofluorescent ring on SW-RAFI (Fig. 2C, upper inset). The macula outside the centrally retained region showed partial demelanization of the RPE in the three patients as evidenced by lower NIR-RAFI signal and visibility of choroidal features; however, this feature did not correspond to RPE atrophy since lipofuscin autofluorescence was retained within the maculas. In P2, there was evidence of RPE atrophy beyond the vascular arcades as evidenced on NIR-RAFI as well as SW-RAFI (Fig. 2C). In all cases, there was interocular symmetry of en face imaging features (data not shown).

Cross-Sectional Retinal Imaging

The retinal lamination of three *TULP1*-RD patients was studied (Fig. 3). Horizontal and vertical cross-sectional images using OCT of the central retina of a normal subject show a foveal depression and orderly retinal layers corresponding to nuclei, synapses and axons (Fig. 3A, upper panels). The ONL (highlighted in blue) is thickest at the fovea and thins with increasing distance from it. Sections from two *TULP1*-RD patients (ages 15 and 25) show that there is ONL at the fovea but it decreases in thickness with increasing eccentricity (Fig. 3A, middle and lower panels). Outer nuclear layer and inner retinal thickness in 3 *TULP1*-RD patients are quantified and plotted in relation to normal limits (Figs. 3B, 3C). In P2 and P3, peak ONL thickness at the fovea is at the lower limit of normal; P1 has reduced thickness at the fovea. Detectable ONL extends to 10 to 15° in the temporal as well as inferior and superior retina in these patients. Inner retinal thickness is normally at a minimum in the fovea. Parafoveal thickening, a feature of normal retina, is also present in the *TULP1*-RD patients. At eccentricities beyond ~10 to 15° eccentric to the fovea, there was abnormal thickening of the inner retina. Such inner retinal abnormalities have been documented in other retinal degenerations.[49–50]

Topographical maps of ONL and inner retinal thickness across an expanse of central retina in *TULP1* retinopathy are shown (Fig. 3D). Normal ONL thickness has a central peak that declines with distance from the fovea. A shallower rate of decline is present in the superior direction (Fig. 3D, upper left panel, inset). In P1, the 15-year-old *TULP1*-RD patient, there is a relatively small region centered on the fovea with retained

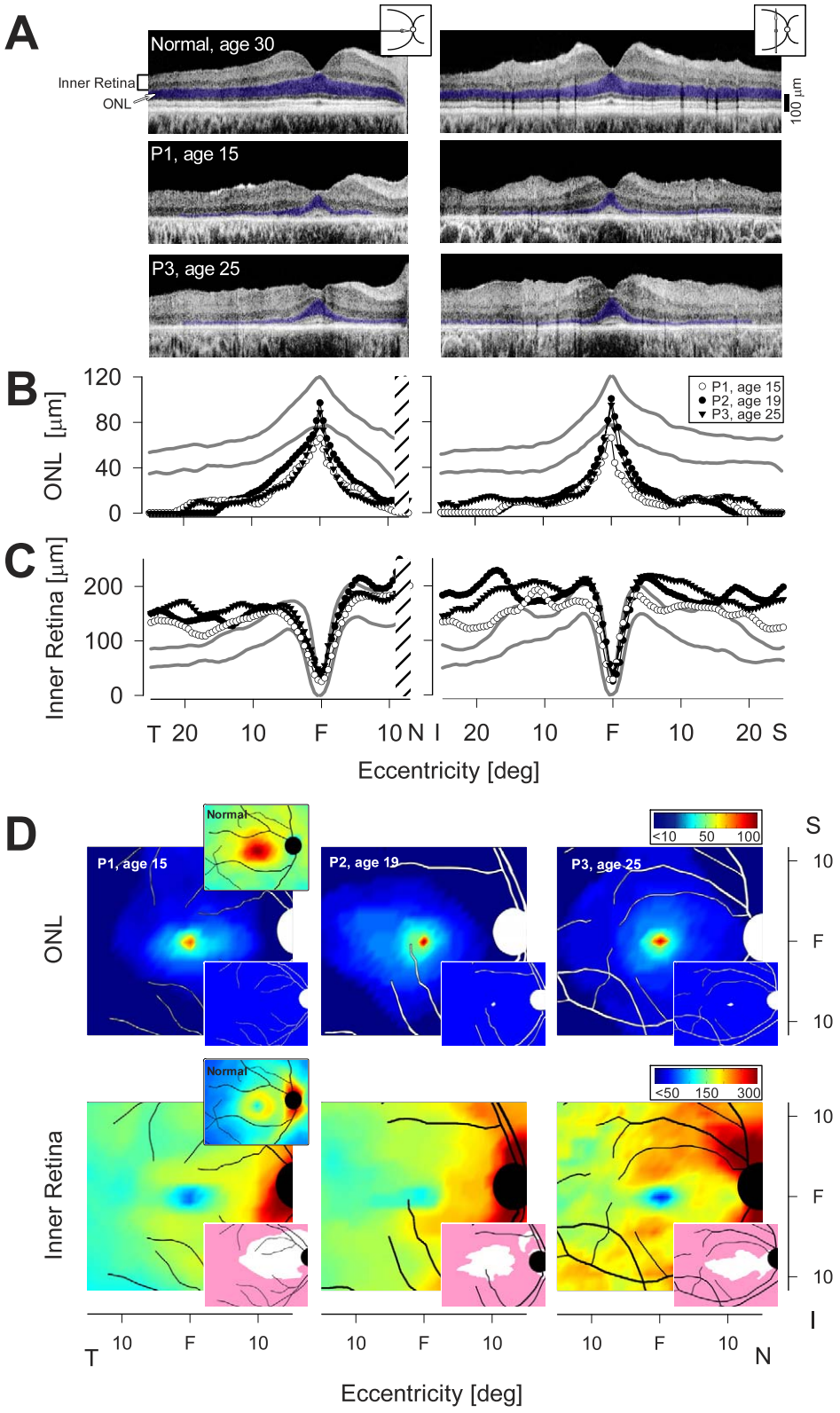

Figure 3. Retinal laminar architecture in *TULP1*-RD patients. (**A**) Cross-sectional OCT images along the horizontal and vertical meridians through the fovea in a normal subject are compared with those of two patients with *TULP1*-RD. Inner retina and ONL are defined at the left edge of the normal image. The ONL is highlighted in *blue*. (**B**) Thickness profiles of ONL in 3 patients ranging in age from 15 to 25 years (symbols identified in key). *Gray lines* define normal limits (mean ± 2 SD; $n = 15$, ages 8–62). Hatched area represents the blind spot. (**C**) Inner retinal thickness profiles for the same 3 patients. (**D**) Thickness topography maps in the central retina of 3 patients (P1–P3) for ONL and inner retina mapped to pseudocolor scales. *Insets to right and above P1 maps:* normal maps for comparison with results from the patients. *Insets to right and below each patient map:* thickness difference maps showing region that is abnormally thinned (*blue*), within normal limits (*white*, defined as mean ± 2 SD), or thickened (*pink*), compared with normal. F, fovea; N, nasal retina; T, temporal retina.

but abnormal photoreceptors; similar regions are detectable in P2 and P3, but the peak thickness in these patients is within the normal limits. The topography of inner retinal laminopathy in the same three patients (Fig. 3D, lower panels) shows there is a central region of inner retina that is normal in thickness but surrounding this region is abnormally thickened retina.

Comparison of *TULP1* Disease With Ciliopathies

Mutation of *TULP1* is considered among the genetic causes of photoreceptor ciliopathy leading to retinal degeneration.[23,51] Ciliopathy genes associated with retinal degeneration have been listed in many published reports.[23–25,51,52] Subcellular localization studies of the gene products contribute to understanding of where in the structure the molecules tend to be found. Also important are studies that determine the function of the molecules and their interactions with other proteins that are disease-associated or not known to be at present.[23–25,51,52] In a review of ciliopathies associated with retinal degeneration,[24] a framework of four ciliary compartments, based mainly on subcellular localization studies of gene products in rod photoreceptors, was defined for the purpose of future investigations of genetic networks: (1) distal cilium or axoneme, (2) connecting cilium/transition zone, (3) basal body, and (4) periciliary complex. Among the retinal diseases associated with each compartment, we chose to compare the impact on structure and function in groups of patients with the following genetic causes (Table): (1) *MAK* (male germ cell-associated kinase); (2) *RPGR* (retinitis pigmentosa GTPase regulator); (3) *BBS1* (Bardet Biedl Syndrome 1); and (4) *USH2A* (Usher Syndrome 2A). The early-onset loss of rod structure and function in *TULP1*-RD directed the analysis to cone structure and function at the fovea. This also presented the opportunity to examine the effects of *TULP1* mutations and the other diseases on cone photoreceptor function and structure; a cone-only region is only able to be studied in humans or non-human primates.

Patients with *MAK*-associated autosomal recessive RP generally have excellent central visual function, even at late ages.[53,54] Foveal ONL thickness in three patients (ages 55, 59, and 72) was within normal limits; COS length was normal or slightly subnormal; and the absolute sensitivities for a long-wavelength target were at the lower limits of normal (Fig. 4A). The *TULP1*-RD patient data (from P1–P3 at ages 15, 19, and 25, respectively) pose a contrast to those of the *MAK*-RP patients (Fig. 4A): whereas cone ONL is normal or near normal, COS are below normal limits (ranging from 66%–79% of mean normal). Foveal cone sensitivity in *TULP1*-RD is markedly reduced; and barely detectable in one patient (P2). The most common molecular cause of X-linked retinal degenerations, *RPGR*, was studied in a group of 16 patients (ages 7–61). There was a spectrum of foveal ONL thicknesses from normal to abnormally reduced; COS length in these patients were mainly abnormal, but to different extents. Cone sensitivities were mildly to severely abnormal. A range of structural and functional abnormalities was also evident in the 7 patients with mutations in *BBS1* (ages 16–29) and six patients with *USH2A* (ages 24–81; Fig. 4A).

Are the disease effects on human cone photoreceptors similar or different in the five genotypes studied? Loss of photoreceptor structure is the underlying basis for loss of photoreceptor function in many retinopathies throughout the course of these diseases or only as a late manifestation in some entities. The patients with *TULP1* mutations appeared to have relatively preserved foveal structures but severe early-onset visual function impairment (Fig. 4A). These observations led to comparisons between the *TULP1*-RD patient results and results from other genotypes. First, we selected data from patients with other genotypes ($n = 9$) that were similar in foveal structure to that of the three *TULP1*-RD patients (Fig. 4B). We defined structure as the product of ONL thickness (a surrogate for photoreceptor numbers) and COS length (surrogate for opsin molecules within each retained photoreceptor) at the fovea.[55,56] The mean visual sensitivity of *TULP1*-RD, however, was significantly lower than that of the nine ciliopathy patients with other mutations (Mann-Whitney rank sum test, $P = 0.016$). Second, we plotted all the structure-function data from the different genotypes and applied a simple linear model which has been used to describe this relationship in various retinal degenerations.[21,50,55–59] Most of the previous studies of human retinal disease have modeled rod photoreceptors and rod vision with only a rare attempt to use cone parameters.[21,55–57] Despite the different compartment assignments of the four cilial genes causing disease, the results indicate that all were behaving similarly and like a pure photoreceptor degeneration. That is, visual sensitivity was reduced linearly with quantum catch. Of interest, the *MAK*–RP patients were nearly normal, suggesting that a disease effect from this gene product may not have a primary impact on human cone cilial structure or function. The *TULP1*-RD patient data differed from the others and fell outside of the 95% confidence interval of the normal variability (Fig. 4C). Inner segment lengths tended to be shorter in *TULP1*-RD ($n = 3$, mean $\pm$ SD $= 29.0 \pm 6.4$ μm) than in other ciliopathy patients ($n = 9$, 33.8 ± 3.7 μm) and normal subjects ($n = 11$, 34.2 ± 2.7 μm), but differences between the three groups did not reach statistical significance (ANOVA, $P = 0.106$). Taken together, the results support the observation that there is a greater degree of dysfunction than could be explained by the loss of cone nuclei and shortening of cone outer segments in *TULP1*-RD.

Discussion

The earliest reports of mutations in the *TULP1* gene described the associated disease as a form of arRP.[4–6] An important issue at the time was whether *TULP1* mutations would cause a syndromic disorder, considering a recessive mutation in the *Tubby* gene in mice was associated not only with retinal degeneration but also with obesity, cochlear abnormalities, and diabetes.[60,61] *TULP1* caused a non-syndromic retinal degeneration and further details emerged over subsequent years. Our study of 16 homozygotes (ages 9–42) with a *TULP1* splice site mutation (IVS14+1 G>A) in two extended Dominican pedigrees indicated that the disease in this population was best considered a form of LCA or EORD.[7] From 2000 to the present day, approximately half of the published studies diagnose patients with *TULP1* mutations as having LCA or EORD.[8–13,62–64] The remainder categorize the disease as arRP, but note childhood-onset vision loss and night blindness.[14,62,65–68] Regardless of clinical diagnosis, early-onset night blindness, visual acuity loss and nystagmus are common findings. To our knowledge, there are no reports of patients with *TULP1* mutations who have onset of symptoms in the second or third decades of life. Ophthalmoscopic features reported were those of other widespread retinal degenerations: vessel attenuation, waxy disc pallor, and RPE changes and/or atrophy; less common were mentions of maculopathy and a central retinal annulus of yellow deposits.[4,7,10,12,13,62,63,66,68,69]

As for visual function, there are only five patients in the literature to date with visual acuities between 20/30 and 20/70 at evaluation[14,62,69]; all others had worse than 20/100. Kinetic visual fields (to large bright targets) could be preserved in early childhood, but peripheral field was lost in later life.[4,7,62] Rod and cone function assayed by ERG has mainly shown no detectable responses; there is one mention of a rod-cone

Investigative Ophthalmology & Visual Science

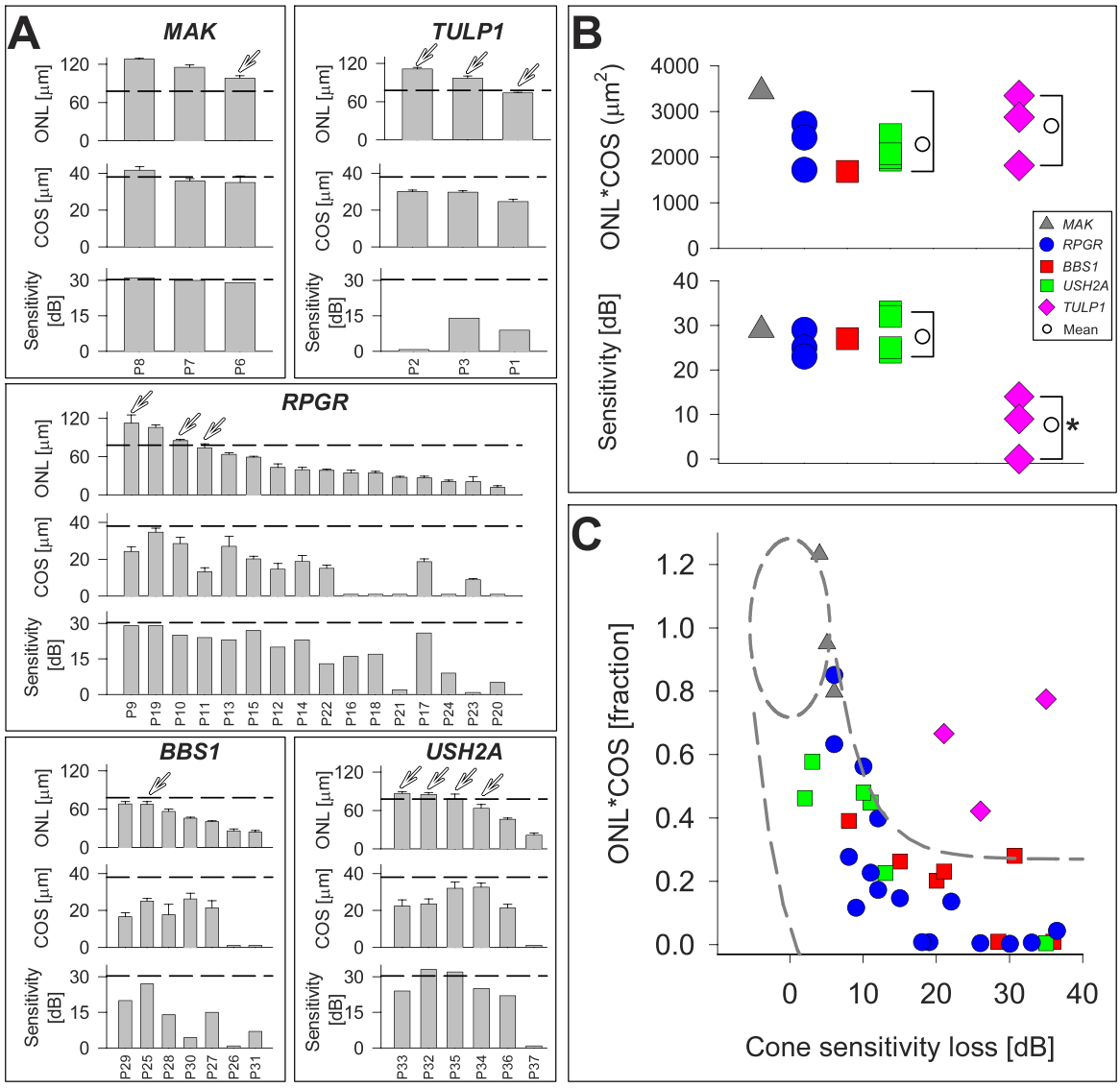

Figure 4. Foveal cone structure and function in *TULP1*-RD compared with four genotypes causing ciliopathies. (**A**) For each of the five different genotypes, three parameters were measured at the fovea: ONL and COS thicknesses, and visual sensitivity (dark-adapted, 650 nm). Patients with *MAK* mutation ($n = 3$; age range, 55–72) had normal or nearly normal structure and function (*top left*). Patients with *RPGR* mutation ($n = 16$; age range, 7-61) had a spectrum of foveal disease (*middle*) as did patients with *BBS1* mutation ($n = 7$; age range, 16-29), and *USH2A* mutations ($n = 6$; age range, 24–81, *bottom right*). Patients with *TULP1*-RD (P1, P2, and P3 at ages 15, 19, and 25, respectively) had severely impaired visual function with normal ONL and some reduction in COS (*top right*). *Error bars*: mean + 2 SE. *Dashed line*: lower limit of normal ($n = 11$; ages 26–62). (**B**) A subset of patients with other ciliopathies ($n = 9$; identified by *arrows* over data in [**A**]) were selected for having similar foveal structure to *TULP1*-RD and visual function was compared. There was a significant difference in the mean visual function between *TULP1*-RD and the patients with other ciliopathies. *Mann-Whitney rank sum test, $P = 0.016$. *Brackets*: range of foveal structure and visual function. (**C**) Relationship between the product of ONL and COS thickness (as a fraction of normal mean) and visual function (cone sensitivity loss) at the fovea in all patients sampled. Normal variability is described by an ellipse encircling the 95% confidence interval of a bivariate Gaussian distribution. *Dashed lines* delimit the region of uncertainty that results by translating the normal variability along the idealized model for pure photoreceptor degenerations. Results in patients with *MAK*, *RPGR*, *BBS1*, and *USH2A* mutations were within the limits predicted by the model. Patients with *TULP1* mutations were outside the confidence limits of the model, showing greater visual dysfunction than anticipated for the measured foveal structure.

pattern.[62] Dark-adapted two-color perimetry in our study of the Dominican population indicated no measurable rod function; the retained central vision was cone-mediated. There were also microvolt-level cone flicker ERGs remaining in some of these patients.[7] Microstructure by OCT is not well described in the literature, but there is a scan (not foveal) in an 8-year-old patient with severe visual loss showing retinal thinning which was attributed to outer retinal disease; an annulus of increased fundus autofluorescence around the fovea was also documented.[10] Recently, *TULP1*-RD was reported to manifest as arCD (cone dystrophy) or arCRD (cone-rod dystrophy).[15] Two unrelated patients with this rare presentation were homozygotes carrying c.1258C > A *TULP1* mutation (p.R420S). A total of 30 disease-associated *TULP1* mutations have been identified to date (summarized in Supplementary Fig. S1). A recently-reported mutation (D94Y) is the only missense mutation located outside of the tubby domain.[64]

How does the current study add to the understanding of the phenotype of patients with *TULP1* mutations? Serial kinetic field data, over 5 to 10 years in some of the patients, indicate

that the peripheral visual loss can be rapid in the *TULP1* genotypes we investigated. Dark-adapted chromatic perimetry confirms our previous measurements in Dominican patients[7] and demonstrates that only cone function is present even in the first decade of life, and it is very diminished in sensitivity. Surprisingly, the small islands of impaired central cone function correspond to measurable and near normal foveal cone photoreceptor structure by OCT and preserved RPE by AF imaging. At greater eccentricities with no measurable function, there is no measurable ONL. At these eccentricities, there is increased inner retinal thickening, a surrogate marker for retinal remodeling in response to loss of photoreceptors.[49,50]

Does the *TULP1* human disease relate to results from the *Tulp1* knockout mouse model? Among the tubby family of proteins,[60] TULP1 was only expressed in photoreceptors.[16] The *tulp1*$^{-/-}$ mouse had a retinal degeneration phenotype with inner and outer segment abnormalities by age 3 weeks. Comparison of effects on cones in the *tulp1*$^{-/-}$ retinas with those in a *rhodopsin* mutant mouse suggested a role for tulp1 in both rods and cones and that cone disease was not simply secondary to rod loss. Extracellular vesicles accumulated around the inner segments and a defect in transport of opsin to the outer segments was proposed.[16] Localization studies of TULP1 in postmortem human retinas at fetal ages indicated strongly positive immunolabeling of immature cones in the central retina by 17 weeks; in contrast, rods were only weakly reactive at these early ages. Postnatal to adult retinas showed prominent TULP1 reactivity in cone and rod inner segments, cell bodies and synapses. The results led to the hypothesis that both cones and rods are affected early in human retinal development.[70] Evidence for photoreceptor synaptic abnormalities in *tulp1*$^{-/-}$ mice has been provided, suggesting that multiple sites in the photoreceptors are affected by tulp1 deficiency.[18,19]

The results in *TULP1*-RD patients in the current study showed a greater degree of dysfunction than anticipated by the measured cone photoreceptor structure—a foveal dissociation of function from structure. This was unlike the function-structure relationships in four other retinal degenerations, all considered ciliopathies,[23–25,51,52] which were more in keeping with a pure photoreceptor degeneration, i.e., the sensitivity to light would be proportional to quantal absorption, as estimated by the number of photoreceptors and their outer segment length. The *TULP1*-RD result showed a resemblance to that previously measured in foveas of *RPE65*-LCA[21,57] where the pathophysiology is thought to involve a substantial reduction in chromophore production.[71] There was also similarity to the results measured in extrafoveal rods of CSNB caused by *NYX* or *CACNA1F* mutations.[58] The pathophysiology of the latter two diseases is thought to localize at the synapses between photoreceptors and bipolar cells.[72,73]

The *TULP1*-RD result demonstrating a dissociation of function and structure at the fovea could be consistent with many different mechanisms. One choice is a relative lack of opsin within the cone outer segments due to reduced transport function along the cone cilia in this primary ciliopathy. Another choice involving downregulation of photoreceptor metabolism associated with relative shortening of the inner segments in patients finds no support in *tulp1*$^{-/-}$ mouse with normal inner segment organelles and mitochondria.[18] Alternatively, it may be greater dysfunction due to early synaptic abnormalities as detected in *tulp1*$^{-/-}$ mice.[19] The early-onset nystagmus in the patients is consistent with cone dysfunction preceding the retinal degeneration, as was the conclusion in the *tulp1*$^{-/-}$ mouse studies. What is the therapeutic potential for this severe retinopathy? The restricted central islands of cone structure may be approachable by an intravitreal gene delivery, given further evidence of the feasibility of this strategy.[74,75] The greatest challenge may be to treat a cone photoreceptor disease with multiple sites of dysfunction.[18,19]

Acknowledgments

Supported by Foundation Fighting Blindness; Hope for Vision; Macula Vision Research Foundation and The Chatlos Foundation, Inc.; National Eye Institute (National Institutes of Health, Department of Health and Human Services) Grant R01 EY017549.

AVC is an RPB Senior Scientific Scholar.

Disclosure: **S.G. Jacobson**, None; **A.V. Cideciyan**, None; **W.C. Huang**, None; **A. Sumaroka**, None; **A.J. Roman**, None; **S.B. Schwartz**, None; **X. Luo**, None; **R. Sheplock**, None; **J.M. Dauber**, None; **M. Swider**, None; **E.M. Stone**, None

References

1. North MA, Naggert JK, Yan Y, Noben-Trauth K. Molecular characterization of *TUB*, *TULP1*, and *TULP2*, members of the novel tubby gene family and their possible relation to ocular diseases. *Proc Natl Acad Sci USA*. 1997;94:3128–3133.
2. Knowles JA, Shugart YY, Banerjee P, et al. Identification of a locus, distinct from *RDS*-peripherin, for autosomal recessive retinitis pigmentosa on chromosome 6p. *Hum Mol Genet*. 1994;3:1401–1403.
3. Shugart YY, Banerjee P, Knowles JA, et al. Fine genetic mapping of a gene for autosomal recessive retinitis pigmentosa on chromosome 6p21. *Am J Jum Genet*. 1995;57:499–502.
4. Banerjee P, Kleyn PW, Knowles JA, et al. *TULP1* mutation in two extended Dominican kindreds with autosomal recessive retinitis pigmentosa. *Nat Genet*. 1998;18:177–179.
5. Hagstrom SA, North MA, Nishina PL, et al. Recessive mutations in the gene encoding the tubby-like protein *TULP1* in patients with retinitis pigmentosa. *Nat Genet*. 1998;18:174–176.
6. Gu S, Lennon A, Li Y, et al. Tubby-like protein-1 mutations in autosomal recessive retinitis pigmentosa. *Lancet*. 1998;351:1103–1104.
7. Lewis CA, Batlle IR, Batlle KGR, et al. Tubby-like protein 1 homozygous splice-site mutation causes early-onset severe retinal degeneration. *Invest Ophthalmol Vis Sci*. 1999;40:2106–2114.
8. Hanein S, Perrault I, Gerber S, et al. Leber congenital amaurosis: comprehensive survey of the genetic heterogeneity, refinement of the clinical definition, and genotype-phenotype correlations as a strategy for molecular diagnosis. *Hum Mutat*. 2004;23:306–317.
9. den Hollander AI, van Lith-Verhoeven JJ, Arends ML, et al. Novel compound heterozygous *TULP1* mutations in a family with severe early-onset retinitis pigmentosa. *Arch Ophthalmol*. 2007;125:932–935.
10. Mataftsi A, Schorderet DF, Chachoua L, et al. Novel *TULP1* mutation causing Leber congenital amaurosis or early onset retinal degeneration. *Invest Ophthalmol Vis Sci*. 2007;48:5160–5167.
11. Abbasi A, Garzozi H, Ben-Yosef T. A novel splice-site mutation of *TULP1* underlies severe early-onset retinitis pigmentosa in a consanguineous Israeli Muslim Arab family. *Mol Vis*. 2008;14:675–682.
12. Li Y, Wang H, Peng J, et al. Mutation survey of known LCA genes and loci in the Saudi Arabian population. *Invest Ophthalmol Vis Sci*. 2009;50:1336–1343.
13. Ajmal M, Khan MI, Michael S, et al. Identification of recurrent and novel mutations in *TULP1* in Pakistani families with early-onset retinitis pigmentosa. *Mol Vis*. 2012;18:1226–1237.

14. Kannabiran C, Singh H, Sahini N, et al. Mutations in *TULP1*, *NR2E3*, and *MFRP* genes in Indian families with autosomal recessive retinitis pigmentosa. *Mol Vis*. 2012;18:1165–1174.
15. Roosing S, van den Born LI, Hoyng CB, et al. Maternal uniparental isodisomy of chromosome 6 reveals a *TULP1* mutation as a novel cause of cone dysfunction. *Ophthalmology*. 2013;120:1239–1246.
16. Hagstrom SA, Duyao M, North MA, Li T. Retinal degeneration in *tulp1-/-* mice: vesicular accumulation in the interphotoreceptor matrix. *Invest Ophthalmol Vis Sci*. 1999;40:2795–2802.
17. Ikeda S, Shiva N, Ikeda A, et al. Retinal degeneration but not obesity is observed in null mutants of the tubby-like protein 1 gene. *Hum Mol Genet*. 2000;9:155–163.
18. Grossman GH, Watson RF, Pauer GJ, et al. Immunocytochemical evidence of Tulp1-dependent outer segment protein transport pathways in photoreceptor cells. *Exp Eye Res*. 2011;93:658–668.
19. Grossman GH, Pauer GJT, Narendra U, et al. Early synaptic defects in *tulp1-/-* mice. *Invest Ophthalmol Vis Sci*. 2009;50:3074–3083.
20. Caberoy NB, Zhou Y, Li W. Tubby and tubby-like protein 1 are new MerTK ligands for phagocytosis. *EMBO J*. 2010;29:3898–3910.
21. Jacobson SG, Aleman TS, Cideciyan AV, et al. Identifying photoreceptors in blind eyes caused by *RPE65* mutations: prerequisite for human gene therapy success. *Proc Natl Acad Sci USA*. 2005;102:6177–6182.
22. Jacobson SG, Cideciyan AV, Peshenko IV, et al. Determining consequences of retinal membrane guanylyl cyclase (RetGC1) deficiency in human Leber congenital amaurosis en route to therapy: residual cone-photoreceptor vision correlates with biochemical properties of the mutants. *Hum Mol Genet*. 2013;22:168–183.
23. Bramall AN, Wright AF, Jacobson SG, McInnes RR. The genomic, biochemical, and cellular responses of the retina in inherited photoreceptor degenerations and prospects for the treatment of these disorders. *Annu Rev Neurosci*. 2010;33:441–472.
24. Rachel R, Li T, Swaroop A. Photoreceptor sensory cilia and ciliopathies. *Cilia*. 2012;1:1–15.
25. Wheway G, Parry DA, Johnson CA. The role of primary cilia in the development and disease of the retina. *Organogenesis*. 2014;10:1–17.
26. Lujan BJ, Roorda A, Knighton RW, Carroll J. Revealing Henle's fiber layer using spectral domain optical coherence tomography. *Invest Ophthalmol Vis Sci*. 2011;52:1486–1492.
27. Curcio CA, Messinger JD, Sloan KR, et al. Human chorioretinal layer thicknesses measured in macula-wide, high-resolution histologic sections. *Invest Ophthalmol Vis Sci*. 2011;52:3943–3954.
28. Sadigh S, Cideciyan AV, Sumaroka A, et al. Abnormal thickening as well as thinning of the photoreceptor layer in intermediate age-related macular degeneration. *Invest Ophthalmol Vis Sci*. 2013;54:1603–1612.
29. Huang Y, Cideciyan AV, Papastergiou GI, et al. Relation of optical coherence tomography to microanatomy in normal and *rd* chickens. *Invest Ophthalmol Vis Sci*. 1998;39:2405–2416.
30. Aleman TS, Cideciyan AV, Sumaroka A, et al. Retinal laminar architecture in human retinitis pigmentosa caused by *Rhodopsin* gene mutations. *Invest Ophthalmol Vis Sci*. 2008;49:1580–1590.
31. Jacobson SG, Aleman TS, Sumaroka A, et al. Disease boundaries in the retina of patients with Usher syndrome caused by *MYO7A* gene mutations. *Invest Ophthalmol Vis Sci*. 2009;50:1886–1894.
32. Maeda T, Cideciyan AV, Maeda A, et al. Loss of cone photoreceptors caused by chromophore depletion is partially prevented by the artificial chromophore pro-drug, 9-cis-retinyl acetate. *Hum Mol Genet*. 2009;18:2277–2287.
33. Cideciyan AV, Rachel RA, Aleman TS, et al. Cone photoreceptors are the main targets for gene therapy of *NPHP5* (*IQCB1*) or *NPHP6* (*CEP290*) blindness: generation of an all-cone Nphp6 hypomorph mouse that mimics the human retinal ciliopathy. *Hum Mol Genet*. 2011;20:1411–1423.
34. Sakami S, Maeda T, Bereta G, et al. Probing mechanisms of photoreceptor degeneration in a new mouse model of the common form of autosomal dominant retinitis pigmentosa due to P23H opsin mutations. *J Biol Chem*. 2011;286:10551–10567.
35. Jacobson SG, Cideciyan AV, Peshenko IV, et al. Determining consequences of retinal membrane guanylyl cyclase (RetGC1) deficiency in human Leber congenital amaurosis en route to therapy: residual cone-photoreceptor vision correlates with biochemical properties of the mutants. *Hum Mol Genet*. 2013;22:168–183.
36. Cideciyan AV, Hufnagel RB, Carroll J, et al. Human cone visual pigment deletions spare sufficient photoreceptors to warrant gene therapy. *Hum Gene Ther*. 2013;24:993–1006.
37. Hood DC, Lin CE, Lazow MA, et al. Thickness of receptor and post-receptor retinal layers in patients with retinitis pigmentosa measured with frequency-domain optical coherence tomography. *Invest Ophthalmol Vis Sci*. 2009;50:2328–2336.
38. Birch DG, Locke KG, Wen Y, et al. Spectral-domain optical coherence tomography measures of outer segment layer progression in patients with X-linked retinitis pigmentosa. *JAMA Ophthalmol*. 2013;131:1143–1150.
39. Jacobson SG, Cideciyan AV, Aleman TS, et al. Crumbs homolog 1 (*CRB1*) mutations result in a thick human retina with abnormal lamination. *Hum Mol Genet*. 2003;12:1073–1078.
40. Spaide RF, Curcio CA. Anatomical correlates to the bands seen in the outer retina by optical coherence tomography: literature review and model. *Retina*. 2011;31:1609–1619.
41. Kocaoglu OP, Lee S, Jonnal RS, et al. Imaging cone photoreceptors in three dimensions and in time using ultrahigh resolution optical coherence tomography with adaptive optics. *Biomed Opt Express*. 2011;2:748–763.
42. Felberer F, Kroisamer JS, Baumann B, et al. Adaptive optics SLO/OCT for 3D imaging of human photoreceptors in vivo. *Biomed Opt Express*. 2014;5:439–456.
43. Cideciyan AV, Swider M, Aleman TS, et al. Reduced-illuminance autofluorescence imaging in *ABCA4*-associated retinal degenerations. *J Opt Soc Am A Opt Image Sci Vis*. 2007;24:1457–1467.
44. Jacobson SG, Voigt WJ, Parel JM, et al. Automated light- and dark-adapted perimetry for evaluating retinitis pigmentosa. *Ophthalmology*. 1986;93:1604–1611.
45. Roman AJ, Schwartz SB, Aleman TS, et al. Quantifying rod photoreceptor-mediated vision in retinal degenerations: dark-adapted thresholds as outcome measures. *Exp Eye Res*. 2005;80:259–272.
46. Jacobson SG, Roman AJ, Aleman TS, et al. Normal central retinal function and structure preserved in retinitis pigmentosa. *Invest Ophthalmol Vis Sci*. 2010;51:1079–1085.
47. Roman AJ, Cideciyan AV, Aleman TS, Jacobson SG. Full-field stimulus testing (FST) to quantify visual perception in severely blind candidates for treatment trials. *Physiol Meas*. 2007;28:N51–N56.
48. Aleman TS, Lam BL, Cideciyan AV, et al. Genetic heterogeneity in autosomal dominant retinitis pigmentosa with low-frequen-

Investigative Ophthalmology & Visual Science

cy damped electroretinographic wavelets. *Eye*. 2009;23:230–233.

49. Jacobson SG, Cideciyan AV, Sumaroka A, et al. Remodeling of the human retina in choroideremia: rab escort protein 1 (*REP-1*) mutations. *Invest Ophthalmol Vis Sci*. 2006;47:4113–4120.
50. Huang WC, Cideciyan AV, Roman AJ, et al. Inner and outer retinal changes in retinal degenerations associated with *ABCA4* mutations. *Invest Ophthalmol Vis Sci*. 2014;55:1810–1822.
51. Estrada-Cuzcano A, Roepman R, Cremers FP, et al. Non-syndromic retinal ciliopathies: translating gene discovery into therapy. *Hum Mol Genet*. 2012;21:R111–R124.
52. Deretic D, Wang J. Molecular assemblies that control rhodopsin transport to the cilia. *Vision Res*. 2012;75:5–10.
53. Tucker BA, Scheetz TE, Mullins RF, et al. Exome sequencing and analysis of induced pluripotent stem cells identify the cilia-related gene male germ cell-associated kinase (MAK) as a cause of retinitis pigmentosa. *Proc Natl Acad Sci USA*. 2011;108:E569–E576.
54. Stone EM, Luo X, Héon E, et al. Autosomal recessive retinitis pigmentosa caused by mutations in the *MAK* gene. *Invest Ophthalmol Vis Sci*. 2011;52:9665–9673.
55. Rangaswamy NV, Patel HM, Locke KG, et al. A comparison of visual field sensitivity to photoreceptor thickness in retinitis pigmentosa. *Invest Ophthalmol Vis Sci*. 2010;51:4213–4219.
56. Birch DG, Wen Y, Locke K, Hood DC. Rod sensitivity, cone sensitivity, and photoreceptor layer thickness in retinal degenerative diseases. *Invest Ophthalmol Vis Sci*. 2011;52:7141–7147.
57. Jacobson SG, Cideciyan AV, Aleman TS, et al. *RDH12* and *RPE65*, visual cycle genes causing Leber congenital amaurosis, differ in disease expression. *Invest Ophthalmol Vis Sci*. 2007;48:332–338.
58. Jacobson SG, Cideciyan AV, Aleman TS, et al. Usher syndromes due to *MYO7A*, *PCDH15*, *USH2A* or *GPR98* mutations share retinal disease mechanism. *Hum Mol Genet*. 2008;17:2405–2415.
59. Cideciyan AV, Aleman TS, Boye SL, et al. Human gene therapy for RPE65 isomerase deficiency activates the retinoid cycle of vision but with slow rod kinetics. *Proc Natl Acad Sci USA*. 2008;105:15112–15117.
60. Mukhopadhyay S, Jackson PK. The tubby family proteins. *Genome Biol*. 2011;28:225.
61. Borman AD, Pearce LR, Mackay DS, et al. A homozygous mutation in the *TUB* gene associated with retinal dystrophy and obesity. *Hum Mutat*. 2014;35:289–293.
62. den Hollander AI, Lopez I, Yzer S, et al. Identification of novel mutations in patients with Leber congenital amaurosis and juvenile RP by genome-wide homozygosity mapping with SNP microarrays. *Invest Ophthalmol Vis Sci*. 2007;48:5690–5698.
63. McKibbin M, Ali M, Mohamed MD, et al. Genotype-phenotype correlation for Leber congenital amaurosis in northern Pakistan. *Arch Ophthalmol*. 2010;128:107–113.
64. Beryozkin A, Zelinger L, Bandah-Rozenfeld D, et al. Identification of mutations causing inherited retinal degenerations in the Israeli and Palestinian populations using homozygosity mapping. *Invest Ophthalmol Vis Sci*. 2014;55:1149–1160.
65. Paloma E, Hjelmqvist L, Bayés M, et al. Novel mutations in the *TULP1* gene causing autosomal recessive retinitis pigmentosa. *Invest Ophthalmol Vis Sci*. 2000;41:656–659.
66. Singh HP, Jalali S, Narayanan R, Kannabiran C. Genetic analysis of Indian families with autosomal recessive retinitis pigmentosa by homozygosity screening. *Invest Ophthalmol Vis Sci*. 2009;50:4065–4071.
67. Iqbal M, Naeem MA, Riazuddin SA, et al. Association of pathogenic mutations in *TULP1* with retinitis pigmentosa in consanguineous Pakistani families. *Arch Ophthalmol*. 2011;129:1351–1357.
68. Hebrard M, Manes G, Bocquet B, et al. Combining gene mapping and phenotype assessment for fast mutation finding in non-consanguineous autosomal recessive retinitis pigmentosa families. *Eur J Hum Genet*. 2011;19:1256–1263.
69. Kondo H, Qin M, Mizota A, et al. A homozygosity-based search for mutations in patients with autosomal recessive retinitis pigmentosa, using microsatellite markers. *Invest Ophthalmol Vis Sci*. 2004;45:4433–4439.
70. Milam AH, Hendrickson AE, Xiao M, et al. Localization of tubby-like protein 1 in developing and adult human retinas. *Invest Ophthalmol Vis Sci*. 2000;41:2352–2356.
71. Cideciyan AV. Leber congenital amaurosis due to RPE65 mutations and its treatment with gene therapy. *Prog Retin Eye Res*. 2010;29:398–427.
72. Morgans CW, Ren G, Akileswaran L. Localization of nyctalopin in the mammalian retina. *Eur J Neurosci*. 2006;23:1163–1171.
73. Zabouri N, Haverkamp S. Calcium channel-dependent molecular maturation of photoreceptor synapses. *PLoS One*. 2013;8:e63853.
74. Boye SE, Boye SL, Lewin AS, Hauswirth WW. A comprehensive review of retinal gene therapy. *Mol Ther*. 2013;21509–21519.
75. Dalkara D, Byrne LC, Klimczak RR, et al. In vivo-directed evolution of a new adeno-associated virus for therapeutic outer retinal gene delivery from the vitreous. *Sci Transl Med*. 2013;5:189ra76.
76. Huang WC, Wright AF, Roman AJ, et al. RPGR-associated retinal degeneration in human X-linked RP and a murine model. *Invest Ophthalmol Vis Sci*. 2012;53:5594–5608.
77. Azari AA, Aleman TS, Cideciyan AV, et al. Retinal disease expression in Bardet-Biedl syndrome-1 (BBS1) is a spectrum from maculopathy to retina-wide degeneration. *Invest Ophthalmol Vis Sci*. 2006;47:5004–5010.
78. Herrera W, Aleman TS, Cideciyan AV, et al. Retinal disease in Usher syndrome III caused by mutations in the clarin-1 gene. *Invest Ophthalmol Vis Sci*. 2008;49:2651–2660.
79. Schwartz SB, Aleman TS, Cideciyan AV, Windsor EA, Sumaroka A, Roman AJ, Rane T, Smilko EE, Bennett J, Stone EM, Kimberling WJ, Liu XZ, Jacobson SG. Disease expression in Usher syndrome caused by VLGR1 gene mutation (USH2C) and comparison with USH2A phenotype. *Invest Ophthalmol Vis Sci*. 2005;46:734–743.

Investigative Ophthalmology & Visual Science